Engineering Structures 302 (2024) 117442

Contents lists available at ScienceDirect

Engineering Structures

journal homepage: www.elsevier.com/locate/engstruct

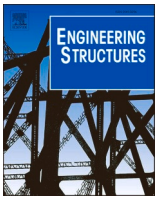

Behaviour and design of duplex stainless steel bolted connections failing in block shear

Yuchen Song [a], Xue-Mei Lin [a,b,c,*], Michael C.H. Yam [a,b], Ke Ke [d], Jia Wang [e]

[a] Department of Building and Real Estate, The Hong Kong Polytechnic University, Hong Kong Special Administrative Region of China
[b] Chinese National Engineering Research Centre for Steel Construction (Hong Kong Branch), The Hong Kong Polytechnic University, Hong Kong Special Administrative Region of China
[c] School of Science and Engineering, University of Dundee, Dundee, Scotland, UK
[d] School of Civil Engineering, Chongqing University, Chongqing, China
[e] School of Transportation, Southeast University, Nanjing, China

ARTICLE INFO

Keywords:
Duplex stainless steel
Bolted connections
Block shear
Anisotropy
Design method
Reliability

ABSTRACT

Duplex stainless steel (DSS) is an emerging construction material for structural engineering, which is featured with high mechanical strength and superior corrosion resistance. Compared with considerable research on DSS structural members, available research is relatively limited for structural joints/connections between these members. In line with this concern, this paper presents a comprehensive experimental and numerical study of duplex stainless steel bolted connections (DSSBCs), focusing on the behaviour and design related to block shear failure. Eleven specimens are tested to investigate the effect of different bolt arrangements on the block shear behaviour. Furthermore, a detailed numerical study was performed as a supplement to the experimental tests, where the anisotropic mechanical properties of DSS are considered in the finite element modelling. Based on the test and analysis results, it is found that the block shear failure mode of DSSBCs resembles that of carbon steel bolted connections, which can be characterised as necking of the tensile section and yielding of the shear sections. Using the experimental and numerical data obtained in this and previous studies, the applicability of various block shear design methods to stainless steel bolted connections is assessed. An updated design method is proposed for predicting the block shear capacity of duplex and austenitic stainless steel bolted connections. A proper partial safety factor/resistance factor is suggested for the proposed method based on the results of reliability analyses.

1. Introduction

In the past few decades, the application of duplex (austenitic-ferritic) stainless steel (DSS) in construction has attracted increasing interests in research and engineering communities [1]. Compared with other widely used categories of stainless steel, i.e. austenitic and ferritic, DSS has higher mechanical strength (especially yield strength) and greater resistance to pitting corrosion [1]. In addition, a newly developed duplex family, known as lean duplex stainless steel, is featured with relatively low nickel content and competitive material cost compared with other stainless steel grades [2]. Due to these benefits, DSS has been applied in a number of iconic construction projects where the life-cycle performance is a major design consideration: representative examples include the Sagrada Família [3] in Barcelona, Spain and the Stonecutters bridge in Hong Kong, China [4]. Despite the great potential of using DSS as a construction material, the design methodology of DSS structures is still not fully addressed in many aspects. A particular uncertainty exists in the structural design of duplex stainless steel bolted connections (lap shear connections), where the potential failures related to net section fracture, bearing (or tear out), block shear and bolt fracture should be properly considered.

Early investigations on the structural behaviour of stainless steel bolted connections (SSBCs) can be traced back to the 1970 s. Errera et al. [5] conducted 25 tests of SSBC between thin-gauge austenitic stainless steel (grade 301) sheets. Four failure modes, namely net section fracture, bearing, tear out and bolt fracture were identified from these tests. SSBCs made of thick (with thickness $t \geq 8$ mm) hot-rolled stainless steel plates were tested by Ryan [6], who incorporated the three major

* Corresponding author at: Department of Building and Real Estate, The Hong Kong Polytechnic University, Hong Kong Special Administrative Region of China.
E-mail address: xlin001@dundee.ac.uk (X.-M. Lin).

https://doi.org/10.1016/j.engstruct.2024.117442
Received 23 August 2023; Received in revised form 3 December 2023; Accepted 31 December 2023
Available online 8 January 2024

stainless steel categories, i.e. austenitic, ferritic and duplex. Their test specimens exhibited bearing, net section and bolt failures. Based on the test data of Ryan [6], Bouchaïr et al. [7] conducted numerical analysis of splice and T-stub connections made of hot-rolled austenitic stainless steel. More specific analyses were performed by Salih et al. [8,9] on bearing and net section failures of austenitic stainless steel bolted connections (ASSBCs). Jiang et al. [10,11] investigated the behaviour of bolted stainless steel connections between angles/channels and plates. Jiang and Zhao [12] introduced a machine learning-assisted design method for stainless steel bolted connections. Experimental tests of cold-formed SSBCs (with relatively thin plates) were reported by Kim et al. [13–16], Talja and Torkar [17], Cai and Young [18–20], dos Santos et al. [21], Sobrinho et al. [22] and Jiang and Zhao [23], covering all stainless steel categories and failure modes. For these thin sheet connections, the curling effect was frequently encountered [13–16,22–24], which has a negative influence on the ultimate capacity. Moreover, the mechanical properties of cold-formed stainless steels are slightly different (typically with higher strength and lower ductility) from those of hot-rolled stainless steels due to the cold working effect. In addition to the investigations of connections at ambient temperature, the high-temperature performance of cold-formed SSBCs was investigated by Cai and Young [25–27]. More recently, Song et al. [28,29] and Stranghöner and Abraham [30,31] studied the failure mode and design of stainless steel bolts subjected to tension, shear and combined loading. Stranghöner et al. [32] and Zheng et al. [33] investigated the behaviour and design of slip-resistant SSBCs. Dobrić et al. [34] examined the net section, bearing and block shear failures of duplex stainless steel bolted connections (DSSBCs) through finite element analysis. In addition to the research on stainless steel lap shear connections, the behaviour of stainless steel beam-to-column joints with bolted connections were recently investigated by Hasan et al. [35,36], Elflah et al. [37–39], Bu et al. [40], Gao et al. [41,42] and Song et al. [43,44,74].

Available test data of SSBCs (lap shear connections) reported in previous studies [5,6,13–17,21,22,45,46] are analysed and visualised in Fig. 1, where a total of 216 individual tests were collected and classified by failure mode (net section, block shear and bearing/tear out failures), material (austenitic, ferritic and duplex) and plate thickness (4 mm is defined as the boundary of thin and thick plates [47]). The tests performed at elevated temperature, as well as those exhibiting bolt failure, were excluded from the analysis considering the specific focus of the present study. From Fig. 1, it can be clearly noticed that most of the existing tests examined the bearing and net section failures of SSBCs, whilst relatively limited tests (16.6%, or 36 tests) were reported on block shear failure. Moreover, these limited tests mainly worked on connections made of thin (cold-formed) stainless steel sheets. Only 5 tests of thick-plate connections (made of 4.5 mm ferritic stainless steel plates) were reported to fail in block shear [17]. It is noteworthy that there is still no test data of austenitic or duplex SSBCs made of hot-rolled plates. Compared with cold-formed plates, thick hot-rolled stainless steel plates are cheaper and more preferable for structural elements in heavy engineering applications Therefore, it will be imperative to conduct more tests to examine the block shear behaviour of hot-rolled stainless steel connections. Moreover, the provisions for SSBCs in recent design guides of stainless steel structures [48,49] basically reproduce the design rules for carbon steel connections [50,51], with some minor modifications to the design for bearing and bolt failure. There is no specific design method for block shear of SSBCs in existing design guides [48,49], which is probably due to the lack of relevant test data and the uncertainty of the block shear behaviour of SSBCs.

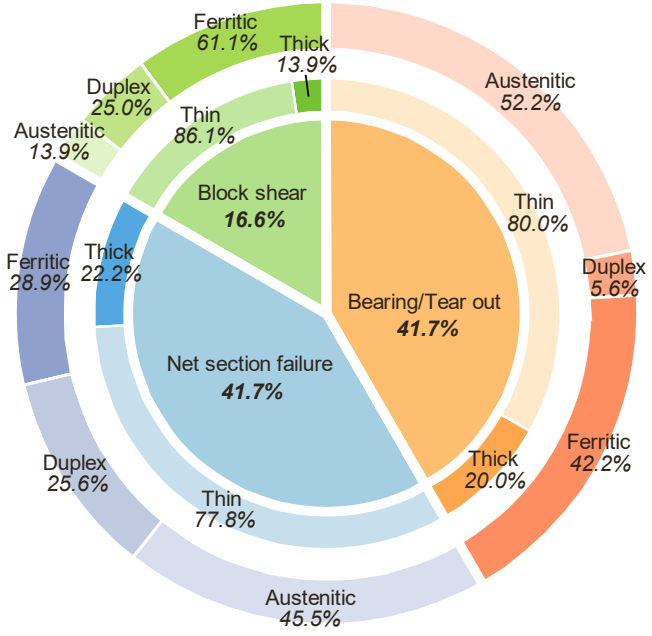

Fig. 1. Statistical analysis of available tests of bolted lap shear connections made of stainless steel.

In line with the above research need, this study investigates the block shear behaviour and design of hot-rolled duplex stainless steel bolted connections (DSSBCs). The block shear behaviour of hot-rolled austenitic stainless steel bolted connections (ASSBCs) was examined in a companion study reported elsewhere [52]. Experimental tests and numerical analysis were performed to examine the block shear behaviour of DSSBCs, which was compared with those of ASSBCs and carbon steel bolted connections. Based on available test and numerical data, various design methods were evaluated and compared for bolted connections made of different materials. A unified design method was subsequently proposed for predicting the ultimate block shear capacity of ASSBCs and DSSBCs. Reliability analyses were performed to determine a proper partial safety factor/resistance factor for the proposed method.

2. Experimental tests

2.1. Test programme

2.1.1. Test design and setup

Thirteen DSSBC specimens were designed and tested, including eleven specimens designed to fail in block shear. The other two specimens were expected to fail in net section fracture and end tear out, which were used for calibrating the finite element models. All the specimens were fabricated from a hot-rolled DSS plate with a nominal thickness of 6 mm. 2205 (EN 1.4462) DSS was selected for the tests, as it is one of the most commonly used duplex grades in practical engineering. The mechanical properties of 2205 DSS are also representative of the entire duplex category.

Fig. 2 shows a typical setup of the connection tests, which were designed to be loaded in double shear to eliminate any eccentricity of loading. Based on the purpose of the tests, the deformation and failure of the connection was designed to concentrate in the 6 mm-thick middle plate (test specimen) made of DSS. High strength steel (with yield strength greater than 1100 MPa) was used to fabricate two 8 mm-thick cover plates, which remained in the elastic regime during testing. Similarly, high strength Grade 12.9 bolts were used for the connections to avoid premature bolt failure. The strength of these bolts is comparable to that of high strength duplex bolts [29] which can be used for connecting duplex members in practical engineering. To exclude the effect of friction (between the cover plates and the middle plate) on the test results, a 7 mm-thick shim plate was inserted between the cover plates to create a gap distance of 1 mm greater than the middle plate thickness. Nuts were installed but kept in a loose condition during testing to avoid closure of the gap. The connections were loaded in a universal testing machine with 500 kN load capacity. The connection deformations

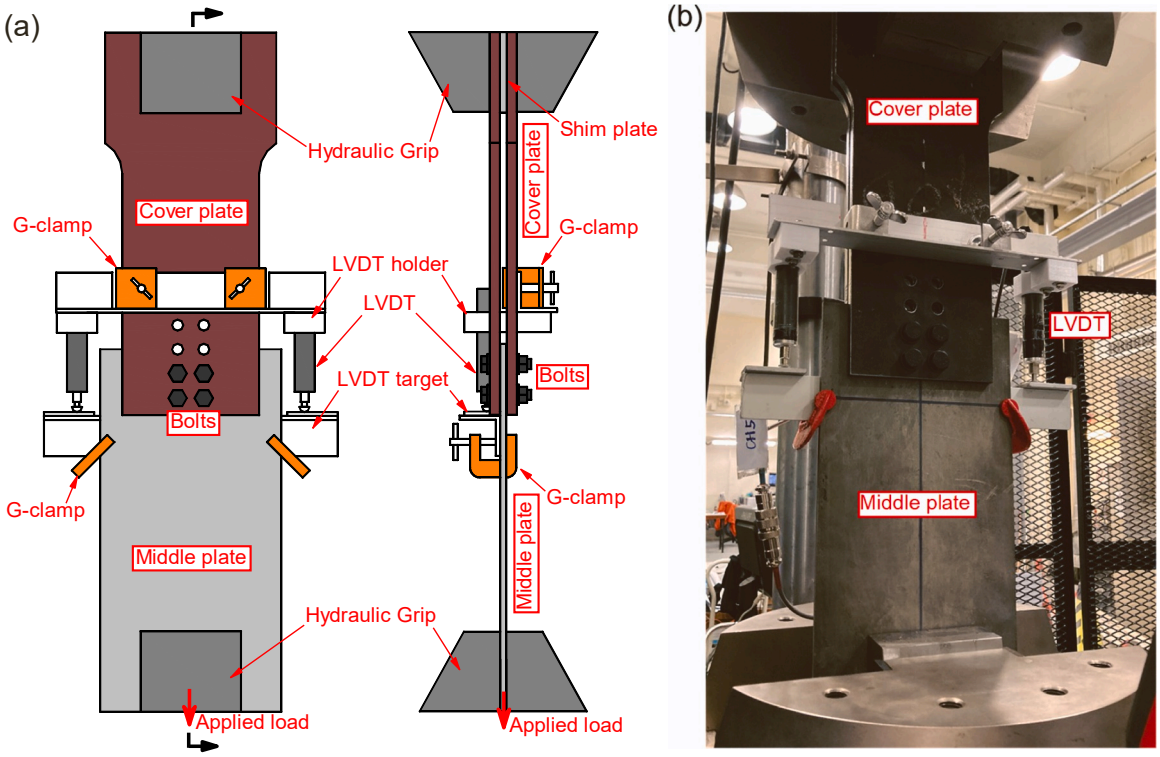

Fig. 2. Setup of connection tests: (a) details of test setup and measuring devices; (b) photo during testing.

(relative displacements of the middle plate and the cover plates) were measured by a pair of linear variable differential transformers (LVDTs) attached to the connection (see Fig. 2).

To achieve the expected failure mode, the geometry and bolt arrangement were carefully designed for each specimen. Table 1 summarises the design variables of all the test specimens, where the implications of different variables are also illustrated. The designation of the specimens was defined to incorporate the values of the main design

Table 1
Summary of specimen design and test results.

Geometry	Specimen	Hole diameter d_0 (mm)	Bolt size	Number of bolt rows n_b	e_1 (mm)	p_1 (mm)	p_2 (mm)	W (mm)	Failure mode	Tested ultimate load R_{test} (kN)	Ultimate loads predicted by FEA R_{FEA}/R_{test}
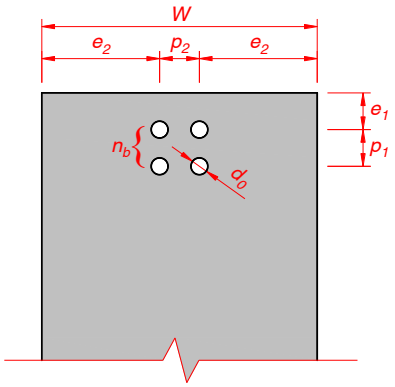	DX-13b2-39_39_39	13	M12	2	39	39	39	78	Net section	237.82	1.003
	DX-13b1-16_00_60			1	16	-	60	142	End tear out	153.23	0.997
	DX-11b1-17_00_26			1	17	-	26	130		152.58	1.011
	DX-11b1-24_00_26			1	24	-	26	130		188.90	1.007
	DX-11b2-17_24_26			2	17	24	26	136		248.80	1.006
	DX-11b2-24_24_26			2	24	24	26	180		286.85	1.002
	DX-11b2-17_31_26	11	M10	2	17	31	26	180		288.77	1.003
	DX-11b2-31_31_26			2	31	31	26	194	Block shear	354.30	1.004
	DX-11b2-17_24_40			2	17	24	40	194		323.15	1.008
	DX-11b3-17_24_26			3	17	24	26	136		332.72	0.995
	DX-11b4-17_24_26			4	17	24	26	194		427.57	0.998
	DX-14b1-22_00_33	14	M12	1	22	-	33	180		193.06	1.008
	DX-14b2-22_31_33	14	M12	2	22	31	33	194		318.22	1.001
	Mean										**1.004**
	CoV										**0.4%**

parameters. For example, the middle part of DX-11b2–17_24_26 means the specimen has 11 mm-diameter bolt holes and 2 rows of bolts (with two bolts in each row, perpendicular to the loading direction); the last six digits divided by "_" represent the pattern of the bolt arrangement (i.e. $e_1 = 17$ mm, $p_1 = 24$ mm, $p_2 = 26$ mm). For specimens with only one row of bolts, the value of p_1 is written as "00" in the designation (e.g. DX-14b1–22_00_33).

2.1.2. Material tests

The mechanical properties of the DSS plate were measured from a series of standard tensile tests [53]. The test samples were extracted from the raw plate along the longitudinal (along the rolling direction, parallel to the loading direction of the connection specimens) and transverse directions of the plate to examine the isotropy of the material. Fig. 3 shows the (engineering) stress-strain curves of the 2205 plate obtained from four individual tensile tests (two for longitudinal and two for transverse directions). Table 2 summarises the key mechanical properties of the material, which were averaged based on the two tests for each direction. The dynamic effect was excluded from the stress-strain curves and mechanical properties following the procedure proposed by Huang and Young [54]. It can be noticed from Fig. 3 and Table 2 that the tested 2205 DSS exhibited relatively large anisotropy: the yield/ultimate strength in the transverse direction is significantly higher (by 7–8%) than that in the longitudinal direction; whilst the ductility (measured by the fracture stain ε_f) in the transverse direction is around 10% lower than that in the longitudinal direction. The elastic modulus measured in the transverse direction is around 17% higher than that measured in the longitudinal direction. The anisotropy of DSS material originates from the microstructure of DSS plates, which composes highly elongated lamellae of ferrite and austenite that possess unusually sharp preferred crystallographic orientations [55]. Similar anisotropy in terms of strength, ductility and elastic modulus were also observed in previous material tests of DSS [56,57]. From the present and past [52,56,57] material tests, it is also noteworthy that the elastic modulus of austenitic/duplex (generally being around 200 GPa) is typically slightly lower than that of common carbon steel.

In Fig. 3 and Table 2, the stress-strain curves and mechanical properties of the tested DSS plate are also compared with those of other structural steels reported in previous studies [52,58], including a grade 304 austenitic stainless steel plate, as well as Q345 and Q960 carbon steel plates. As can be seen, the yield ($F_{0.2}$) and ultimate (F_u) strengths of the DSS (2205) lie in between those of Q345 and Q960 carbon steels. The 304 steel possesses comparable ultimate strength to the DSS, and significantly lower yield strength than the other materials. The resultant ultimate-to-yield strength ratio (F_u/F_y) of the DSS is around 1.34 for both directions, which is slightly higher than those of the carbon steels, and remarkably lower than that of the 304 steel (2.90). The ductility (ε_f) of the 2205 DSS is in between those of the austenitic and carbon steels.

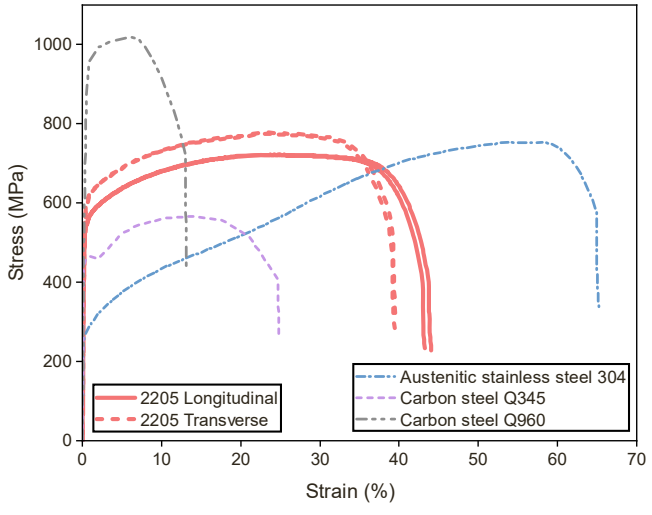

Fig. 3. Stress-strain curves of the duplex stainless steel plate and comparison with other materials.

2.1.3. Loading procedure

To assist the identification of the block shear mode, lines were marked on each specimen before testing, along three critical failure planes (see Fig. 4). These include the net tensile plane along the line passing the centres of the 1st (innermost) row bolt holes, as well as the net and gross shear planes passing the centres and the outer edges of the bolt lines along the loading direction. The connections were loaded monotonically with a stroke rate of 0.15–0.3 mm/min. The loading was paused at 1.5, 3 and 4.5 mm connection displacements to obtain the corresponding static loads. The testing was ceased immediately after reaching the ultimate load, at which the connection was unloaded and dissembled to enable visual inspection of the block shear mode of the middle plate. The connection was subsequently reassembled and reloaded until complete fracture of the middle plate. For most of the specimens, unloading/reloading was conducted once more following a sudden load drop observed from the load-displacement curve. This always corresponded to a major fracture of the middle plate. It was observed in the tests that the unloading and reloading branches of the load-displacement curve before and after each dissembling overlapped satisfactorily for all the specimens. A continuous load-displacement curve can be hence generated by splicing the unloading and reloading curves (see Fig. 5). The load-displacement curves recorded in the tests were converted to the static load-displacement curves following the procedure outlined in Refs. [43,52], as shown in Fig. 5. For the sake of cleanliness, the portions corresponding to pauses and unloading/-reloading were removed from the finalised load-displacement curves (see Fig. 6 for example).

2.2. Test results

2.2.1. Load-displacement response and block shear mode

The (static) load-displacement curves and failure modes (photographed following each unloading and the end of test) of three representative block shear specimens are illustrated in Fig. 6. Fig. 7 shows the test load-displacement curves of all the block shear specimens, with their ultimate loads summarised in Table 1. It was observed that all the block shear specimens failed in a similar manner. At the ultimate load (see State 1 in Fig. 6), all the specimens showed obvious necking along the net tensile plane, and significant shear deformations (indicating yielding of the shear regions) between the net and gross shear planes. This was followed shortly by a sudden drop of load, corresponding to fracture of the net tensile section (State 2 in Fig. 6(a) and (b)). Up to this state, there was no sign of cracking/fracture around the shear planes. At the final failure state (State 3 in Fig. 6(a) and (b), State 2 in Fig. 6(c)), shear fractures formed between the net and gross shear planes, with the net tensile section being pulled apart significantly at the meantime. Thereafter, the load capacity of a connection was practically lost, and the testing was therefore terminated.

The test results of the two specimens that exhibited net section and tear out failures were mainly used for calibrating the numerical model, which will be presented in Section 3.2.

2.2.2. Comparison with austenitic stainless steel and carbon steel bolted connections

The experimental block shear behaviour of DSSBCs was compared with those of ASSBCs and carbon steel bolted connections. Fig. 8(a) shows the load-displacement responses of DSSBC specimen DX-11b2–17_24_26, as well as two carbon steel (Q345 and Q960) [58] and an ASSBC [52] specimens that have the same bolt arrangement as DX-11b2–17_24_26. It is apparent that the deformation capacity (measured by the displacement at the peak load) of the DSSBC specimen

Table 2
Mechanical properties of the tested duplex stainless steel plate (2205) and comparison with other materials.

Steel category	Grade	Nominal plate thickness (mm)	Direction of specimen	Mechanical properties (average values of multiple tests)					
				Elastic modulus E (GPa)	Yield strength $F_{0.2}$ (or F_y) (MPa)	Ultimate strength F_u (MPa)	Strength ratio F_u/F_y	Ultimate strain ε_u (%)	Fracture strain ε_f (%)
Duplex	2205 (EN 1.4462)	6	Longitudinal	186.1	539.2	721.0	1.34	26.1	43.4
			Transverse	217.1	579.4	776.4	1.34	22.8	39.2
Austenitic	304 (EN 1.4301)	6	Longitudinal	201.4	260.8	755.9	2.90	57.6	64.7
Carbon steel	Q345	6	-	210	456	564	1.24	14.2	26.7
	Q960	5	-	203	932	1022	1.10	6.2	14.6

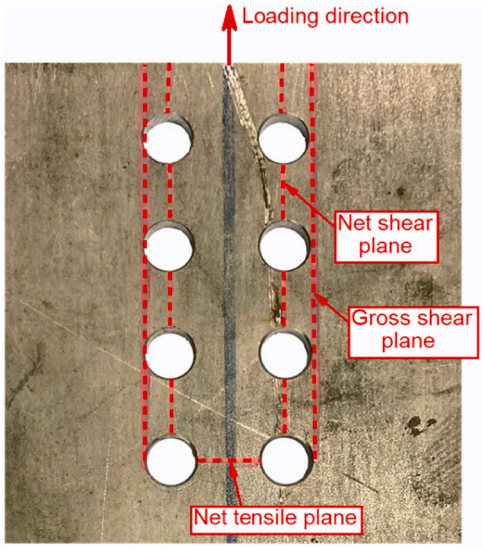

Fig. 4. Failure plane definitions for block shear.

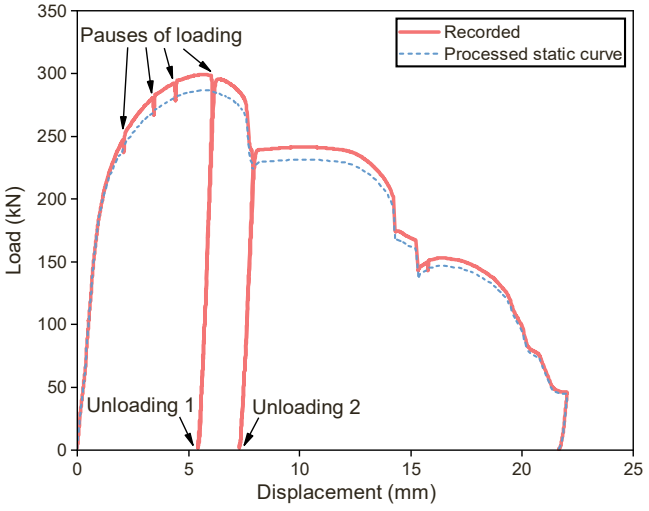

Fig. 5. Loading procedure and processing of load-displacement curve.

is higher than those of the carbon steel specimens, and lower than that of the ASSBC specimen. This echoes the relative ductility of the four materials as shown in Fig. 3 and Table 2. The block shear modes of the four specimens at the peak/ultimate load (PL) and after the sudden fracture (AF) are shown in Fig. 8(b)-(e), where one can see that the block shear modes of the DSSBC and carbon steel specimens are similar (see Fig. 8 (b)-(d)): at the ultimate load, all the specimens exhibited necking of the net tensile section and yielding of the shear sections (tensile necking and shear yielding). The following sudden load drops of these specimens were attributed to fracture of the net tensile section, with no fracture/cracking observed in the shear regions. This block shear mode is actually the one assumed in most of the previous studies [58–63] and design provisions [50,51,64,65] for block shear design of carbon steel bolted connections. Different from the DSSBC and carbon steel specimens, cracking of the shear regions was observed in the ASSBC specimen at the ultimate load, along with necking of the net tensile section (tensile necking and shear cracking, see Fig. 8(e)). Shortly after attaining the peak load, sudden fractures occurred in both the tensile and shear regions, leading to a significant load drop. Moreover, it is worth mentioning that with different bolt arrangements, two more block shear modes (corresponding to the ultimate load) were observed for ASSBCs, namely tensile necking and shear yielding, as well as tensile yielding and shear cracking [52]. The unique block shear modes of ASSBCs compared with their duplex and carbon steel counterparts were deemed to be due to the very high ductility of austenitic stainless steel, which enabled early shear cracking before fracture or even necking of the tensile section.

3. Numerical analysis

3.1. Finite element model

Finite element (FE) models were developed using the ABAQUS software [66] to further examine the block shear behaviour of DSSBCs, and generate more data for the evaluation of design methods. Fig. 9 shows the FE model of connection specimen DX-11b2–24_24_26, which is the one illustrated in the test setup (Fig. 2). Taking advantage of the symmetry, one-fourth of the entire connection was modelled to reduce the computation time. The planes of symmetry (PoS) in YZ and XY planes were restrained against the displacements in X- and Z-directions respectively (see Fig. 9). The load was applied by controlling Y-axis displacements of two reference points labelled as RP1 and RP2, which were coupled with the movements of both ends of the connection through “Rigid body” constraints.

As shown in Fig. 10, a mesh sensitivity analysis was performed on a typical connection model (DX-11b2–24_24_26) to determine an optimum combination of mesh size and element type of the models. Relatively fine meshes (with a minimum mesh size of around 0.1 ×0.4 ×0.5 mm, representing length in loading direction × length in transverse direction × length in thickness direction) with the element type “C3D8I” (3D brick element having 8 integration points) were finally employed for the middle plate, where large plastic deformations and fractures are expected to occur. It was noticed that coarser meshes may not be able to accurately simulate the necking and fracture behaviour of the middle plate in the tensile region (see Fig. 10). On the other hand, finer meshes (with a minimum size of 0.05 ×0.25 ×0.5 mm) led to almost identical simulation results at a much higher computational cost. Coarser meshes (around 2 ×2 ×2 mm) with C3D8R elements (3D brick element having 1 integration point) were employed for the cover plate and bolts that experienced limited deformations. The contact in the normal direction was defined as infinitely rigid. To accurately

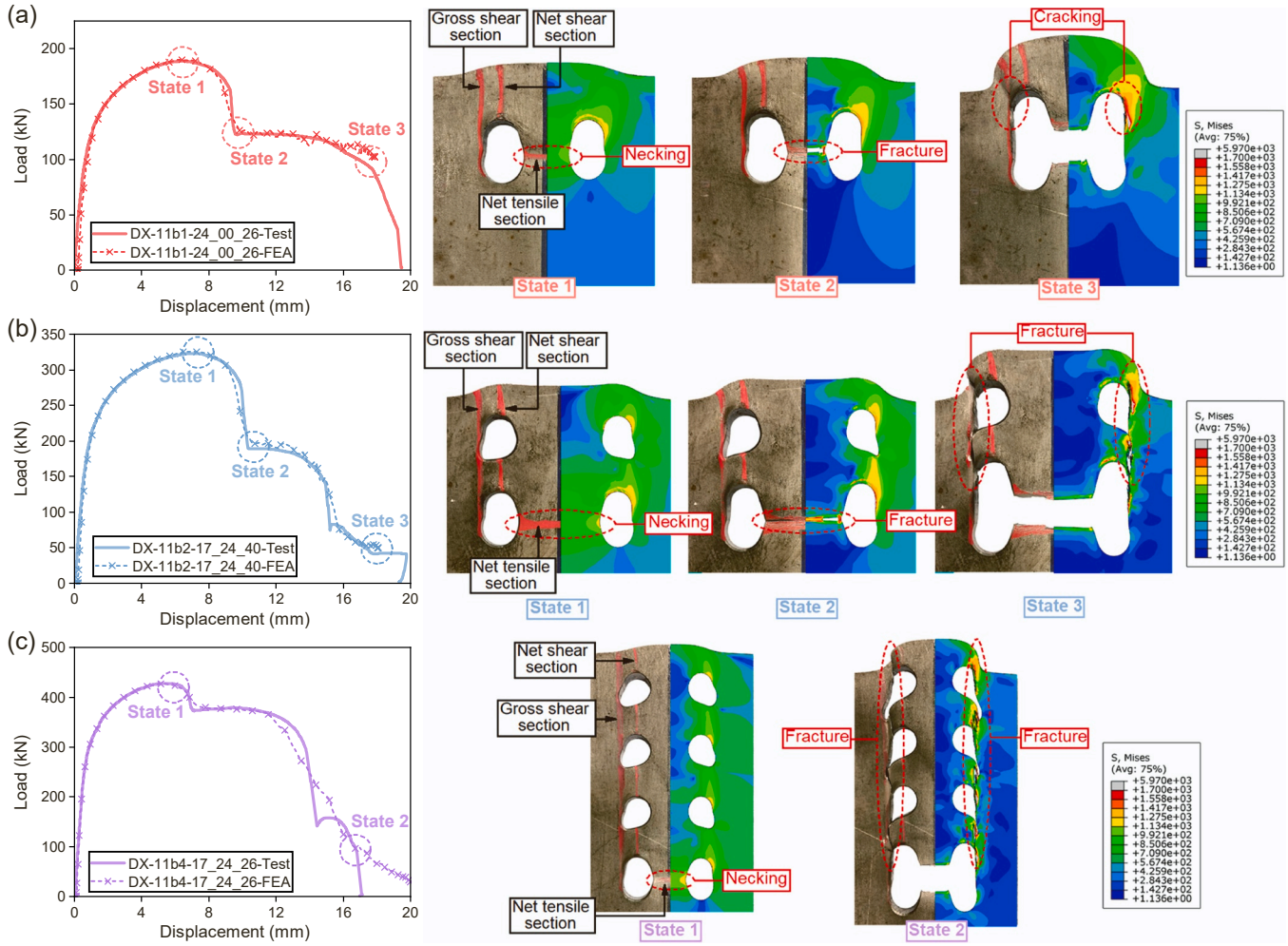

Fig. 6. Typical load-displacement curves and failure modes: (a) Specimen DX-11b1–24_00_26; (b) Specimen DX-11b2–17_24_40; (c) Specimen DX-11b4–17_24_26.

simulate the actual testing condition (described in Section 2.1.1), the friction effect was minimised by modelling the initial gaps between the cover plates and middle plate. The analysis was performed using the ABAQUS/Explicit module. The step time was set as 0.5 s, which is sufficient to ensure a quasi-static loading condition with relatively small kinetic energy (<10% of the internal energy) [66]. A localised mass scaling was assigned to the model (especially the middle plate) to further accelerate the analysis without disturbing the results.

3.2. Modelling of duplex stainless steel material

Accurate modelling of the constitutive and fracture properties of DSS is of paramount importance to correctly simulating the block shear failure of DSSBCs. In Ref. [44], the authors outlined a simple yet satisfactorily accurate framework for modelling the full-range plasticity and fracture of stainless steel with only four parameters. It has been demonstrated that the proposed framework is suitable for ASSBCs [52], where the failure planes are mainly in plane stress states. Within this framework, the uniaxial constitutive relationship of the material is defined by:

$$\begin{cases} \varepsilon_t = \ln(1+\varepsilon), \sigma_t = \sigma(1+\varepsilon) (\varepsilon \le \varepsilon_u) \\ \sigma_t = \sigma_{t,u}\left[w \bullet \exp\left(\varepsilon_t - \varepsilon_{t,u}\right) + (1-w)\right] (\varepsilon > \varepsilon_u) \end{cases} \tag{1}$$

$$w = 1 \Big/ \left[1 + a_1 \left(\varepsilon_t - \varepsilon_{t,u}\right)^{a_2}\right] \tag{2}$$

where σ/ε and σ_t/ε_t are the engineering stress/strain and the corresponding true values. the additional subscript "u" indicates the ultimate stress/strain at the onset of necking. w is a weight average factor determining the stress-strain characteristic in the post-necking range, which is controlled by two parameters a_1 and a_2 calibrated through matching the tested engineering stress-strain curves of tensile coupons with those simulated by finite element analysis (FEA).

Alongside the constitutive model, the criterion proposed by Lee and Wierzbicki [67] is adopted for modelling the fracture behaviour of stainless steel materials:

$$\varepsilon_{pl,f} = \begin{cases} \infty, \eta \le -1/3 \\ \dfrac{C_1}{(1+3\eta)}, -1 \Big/ 3 < \eta \le 0 \\ C_1 + (C_2 - C_1)(3\eta)^2, 0 < \eta \le 1/3 \\ \dfrac{C_2}{3\eta}, \eta > 1 \Big/ 3 \end{cases} \tag{3}$$

Eq. (3) defines the fracture strain $\varepsilon_{pl,f}$ as a function of stress triaxiality η, where the two parameters C_1 and C_2 can be calibrated by two groups of specimens that exhibited shear- and tensile-dominant fractures, respectively. The dependency of Lode angle is not considered in the adopted fracture criterion. As discussed in Ref. [52], the stress states of the middle plates in the considered bolted connections are largely plane stress in the majority of loading. Since the parameters of stress triaxiality and Lode angle are related in a plane stress state, fracture criteria with both triaxiality and Lode angle dependency will reduce to only one independent variable, i.e. with only triaxiality dependency.

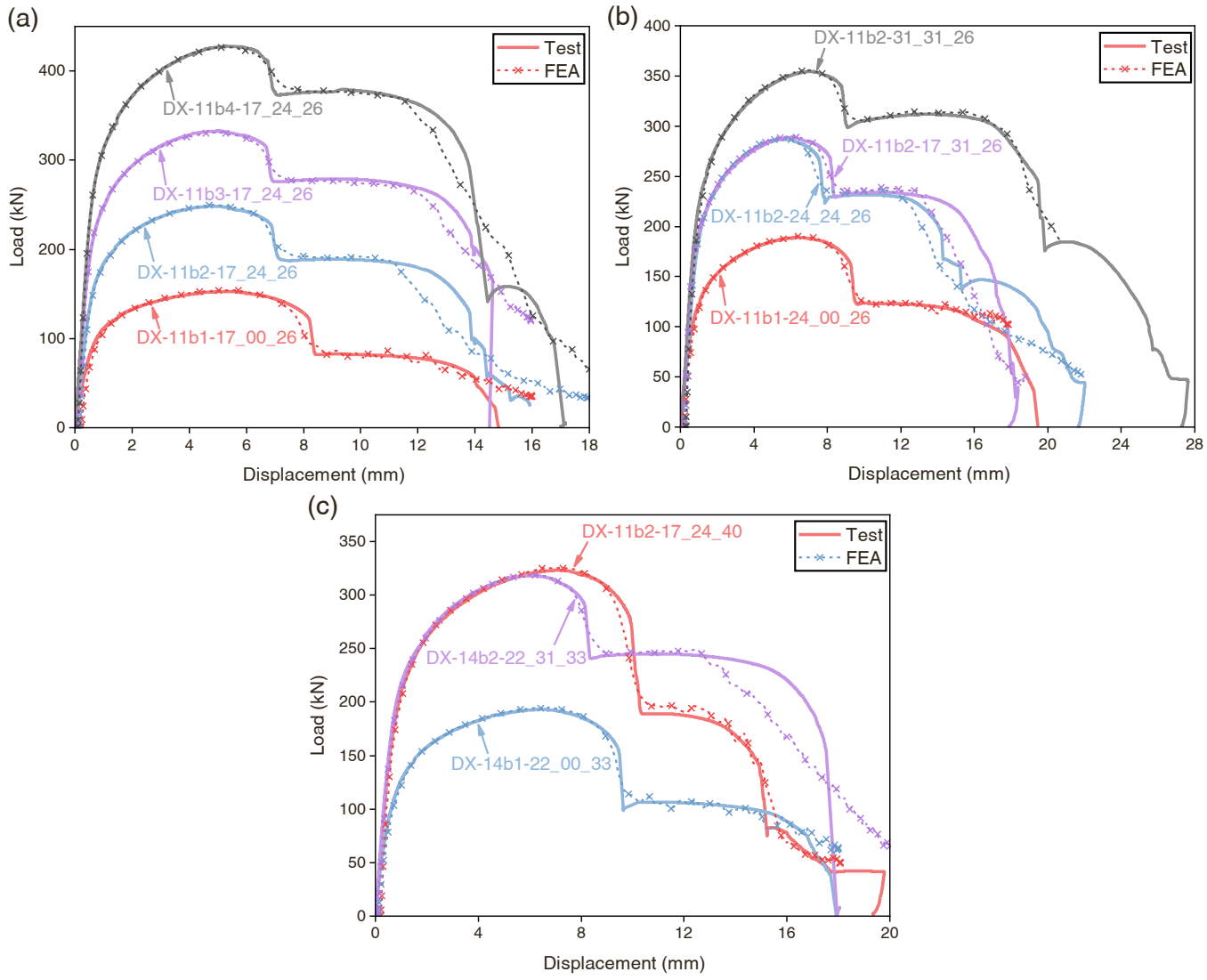

Fig. 7. Test vs. FEA load-displacement curves.

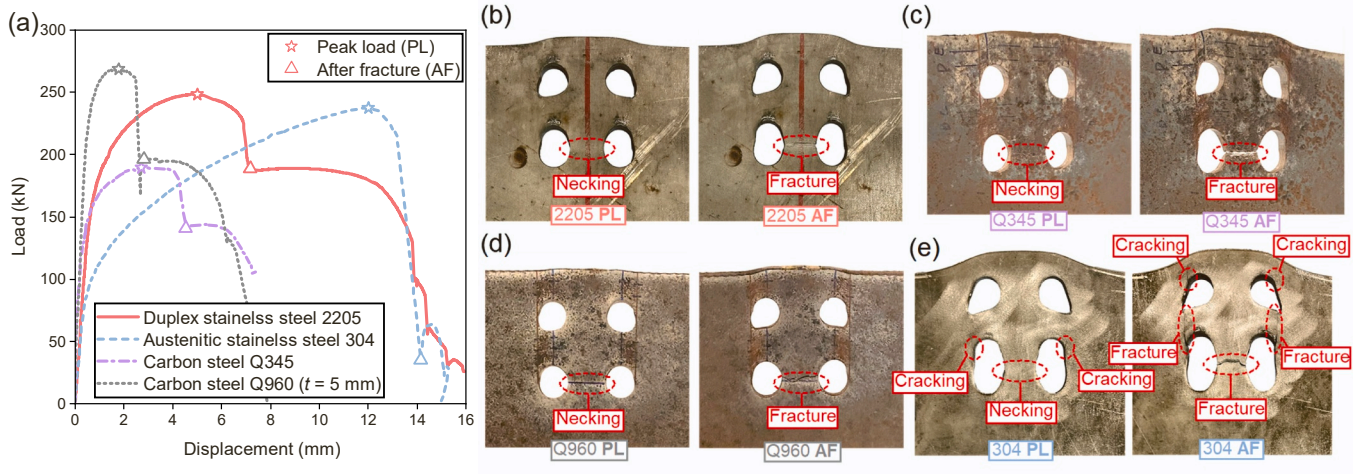

Fig. 8. Comparison of block shear failure modes of different bolted connections: (a) load-displacement curves; (b) failure mode of DSSBC; (c) failure mode of Q345 carbon steel connection; (d) failure mode of Q960 carbon steel connection; (e) failure mode of ASSBC.

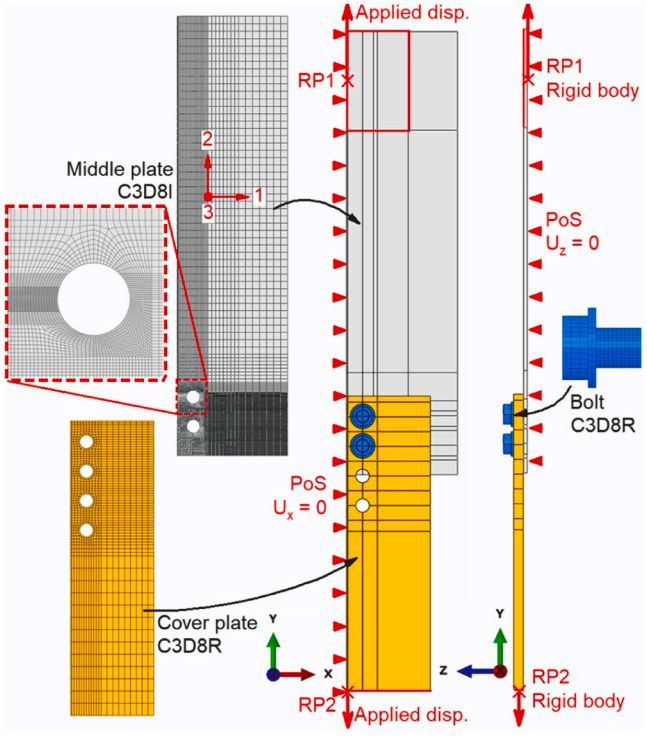

Fig. 9. Illustration of a typical finite element model of DSSBC.

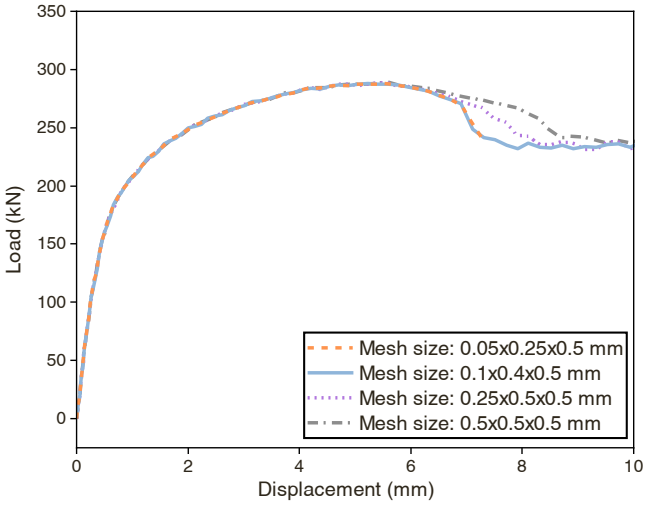

Fig. 10. Mesh sensitivity analysis of the finite element model.

Within the above framework, the plasticity of the material is described by von Mises yield criterion and isotropic hardening. This is appropriate for common carbon steel that can be considered as isotropic material. However, for the DSS investigated in this study, the significant anisotropy in stress-strain characteristic necessitates specific considerations in material modelling. In particular, the Hill yield criterion [68] developed for anisotropic metals was adopted in replacement of the von Mises criterion. The potential function of the Hill criterion, which is an extension of the Mises potential function, is expressed as follows:

$$f(\boldsymbol{\sigma}) = \sqrt{F(\sigma_{22}-\sigma_{33})^2 + G(\sigma_{33}-\sigma_{11})^2 + H(\sigma_{11}-\sigma_{22})^2 + 2L\sigma_{23}{}^2 + 2M\sigma_{31}{}^2 + 2N\sigma_{12}{}^2} \tag{4}$$

where F, G, H, L, M and N are coefficients determining the anisotropy of the yield surface. Neglecting the anisotropy of shear yield stress, the last three constants will be equal to 3/2 and Eq. (4) can be reduced to:

$$f(\boldsymbol{\sigma}) = \sqrt{F(\sigma_{22}-\sigma_{33})^2 + G(\sigma_{33}-\sigma_{11})^2 + H(\sigma_{11}-\sigma_{22})^2 + 3(\sigma_{23}{}^2+\sigma_{31}{}^2+\sigma_{12}{}^2)} \tag{5}$$

$$F = \frac{1}{2}\left(\frac{1}{R_{22}^2}+\frac{1}{R_{33}^2}-\frac{1}{R_{11}^2}\right), G = \frac{1}{2}\left(\frac{1}{R_{33}^2}+\frac{1}{R_{11}^2}-\frac{1}{R_{22}^2}\right), H = \frac{1}{2}\left(\frac{1}{R_{11}^2}+\frac{1}{R_{22}^2}-\frac{1}{R_{33}^2}\right) \tag{6}$$

In Eq. (6), R_{11}, R_{22} and R_{33} are anisotropic yield stress ratios defined by:

$$R_{11} = \frac{\overline{\sigma}_{11}}{\sigma_0}, R_{22} = \frac{\overline{\sigma}_{22}}{\sigma_0}, R_{33} = \frac{\overline{\sigma}_{33}}{\sigma_0} \tag{7}$$

where σ_0 is a reference yield stress. $\overline{\sigma}_{ii}$ is the yield stress when σ_{ii} is the only non-zero stress component. In the present FE models, the orientations 1, 2 and 3 of the DSS plate (middle plate) were defined as shown in Fig. 9. The yield stress measured in direction 2 (rolling/loading direction) was assigned as the reference yield stress σ_0. The input uniaxial stress-strain relationship was hence obtained from the coupon tests of the longitudinal specimens and converted into true values through Eq. (1). Consequently, R_{22} is equal to 1.0. The initial value of R_{11} was determined referring to the ratios of the yield stresses ($F_{0.2}$) and ultimate stresses (F_u) measured in the transverse and longitudinal directions, taken as 1.076. The yield stress ratio in the through-thickness direction (R_{33}) is closely related to the lateral contraction of the material in tension. R_{33} was determined to be 0.9, through a comparison of the tested and FE simulated cross-sectional contractions of the tensile coupons. To exclude the complex effect of necking, such contractions were measured (measured by a caliper in testing after the end of loading) at the edges of the gauge length well away from the necking region, where the contractions were solely caused by anisotropic plastic flow in the pre-necking range. It was observed that the selected combination of yield stress ratios (1.076, 1.0 and 0.9 for R_{11}, R_{22} and R_{33}) produced a satisfactory agreement of the tested and simulated contractions in the transverse and through-thickness directions. In addition, the selected R_{33} also led to an accurate simulation of the failure mode (especially the transverse and through-thickness contraction of the net tensile region after fracture) of the tensile specimen (DX-13b2–39_39_39), as shown in Fig. 11(a). It is worth mentioning that the lower yield stress ratio in the through-thickness direction compared with those in the rolling and transverse directions may be explained by the unique microstructure of duplex stainless steel with highly elongated lamellae [55], It may be postulated that "squeezing" the stacks of lamellae to yielding in the through-thickness direction requires less force compared with "stretching" the lamellae to yielding in the rolling/transverse direction. However, direct investigation on this behaviour was not found in literature and more research is probably required.

The other material parameters (a_1, a_2, C_1, and C_2) were calibrated by specimens DX-13b2–39_39_39 (tensile specimen) and DX-13b1–16_00_60 (shear specimen) that failed in net section fracture and end tear out respectively, where the stress states are representative of those in the tensile and shear failure regions of a block shear specimen. The constitutive parameters a_1 and a_2 were first determined by comparing the post-peak branches of the test and simulated load-

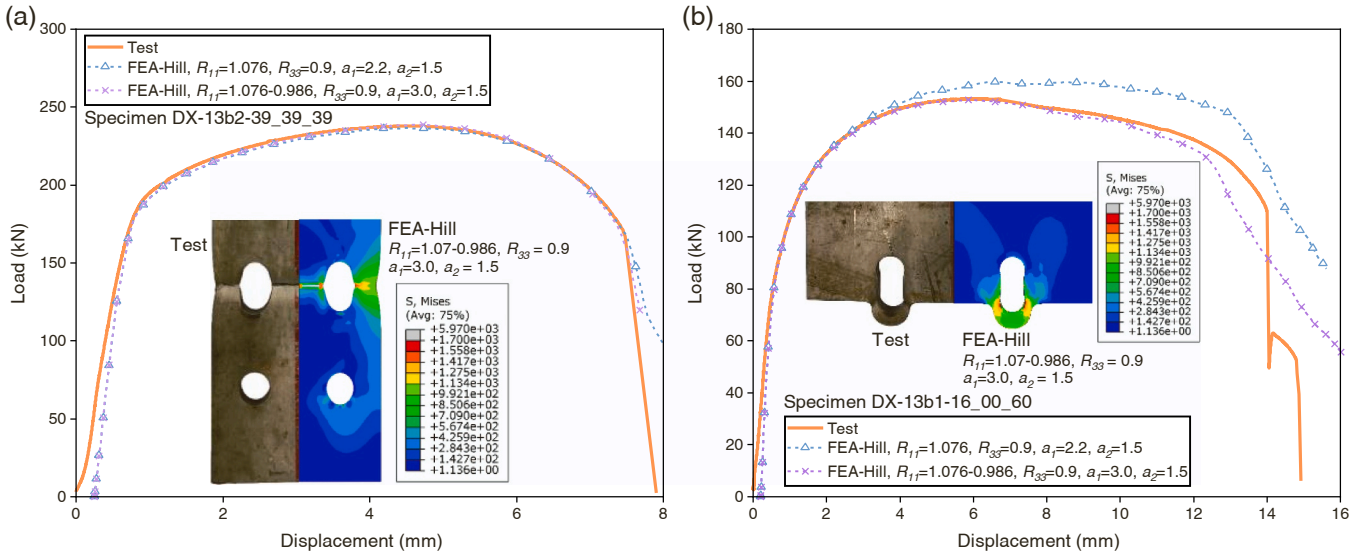

Fig. 11. Calibration of the material parameters by (a) tensile specimen; (b) shear specimen.

displacement curves (a_1=2.2, a_2=1.5). However, it was noted that the constitutive parameters calibrated for the tensile specimen were not equally suitable for the shear specimen: the simulated loads appeared to be higher than the test values (see Fig. 11(b)). This might be due to the variation of the anisotropic yield stress ratio R_{11} with the development of plastic strain. The shear specimen is particularly affected by R_{11} since it is mainly stressed in direction 1. After a series of trial-and-error, R_{11} was set to reduce linearly from 1.076 to 0.986 with the equivalent plastic strain (PEEQ) increasing from 0 to 0.2. For PEEQ greater than 0.2, R_{11} maintains constant at 0.986. With the updated R_{11}, a_1 and a_2 were recalibrated as 3.0 and 1.5. As shown in Fig. 11, the updated material parameters lead to consistently good predictions for both the tensile and shear specimens. Finally, the fracture parameters C_1 (1.5) and C_2 (4.5) were determined by matching the test and simulated fractures of the tensile and shear specimens.

3.3. Model validation

The developed FE models and the calibrated material parameters were validated by the eleven block shear specimens. Fig. 6 compares the test and FEA load-displacement curves and block shear modes of three typical specimens. The test/FEA load-displacement curves of all the specimens are shown in Fig. 7. As can be seen, the load-displacement response and failure mode of the tested DSSBCs were accurately simulated by the developed FE models. The ratios of the FEA and test ultimate loads are given in Table 1, with an average ratio of 1.004 and a coefficient of variation (CoV) of 0.4%.

3.4. Further analysis and discussions

Using the developed FE models, further analyses were performed to cover more design parameters of DSSBCs. Table 3 summarises the adopted parameters for these (76 in total) analyses/models. It has been demonstrated in a previous study [52] that the middle plate thickness and bolt hole diameter have very little effect on the block shear behaviour. These parameters were hence maintained constant (6 mm for plate thickness, 11 mm for hole diameter) for all the models. The materials of the middle plate, cover plates and bolts (M10 G12.9) are consistent with those in the tests. The main parameters varied in the analyses include the number of bolt rows and the bolt arrangement (e_1, p_1 and p_2, with their implications illustrated in Table 1).

The results of 76 FEA (summarised in Table 3) confirmed again that the only block shear mode (corresponding to the ultimate load) of DSSBCs is tensile necking and shear yielding (as shown in Fig. 6). To further examine the load-carrying behaviour of DSSBCs failing in block shear, the load-displacement curves obtained from the FEA were split into those contributed by the tensile and shear sections (see Fig. 12). The derived loads carried by the tensile section (tensile loads) were compared with the theoretical ultimate resistance of the net tensile section, i.e. $R_{nt} = F_u A_{nt}$ (A_{nt} is the area of the net tensile section, F_u takes the ultimate strength in the longitudinal direction). The loads carried by the shear sections (shear loads) were compared with the theoretical ultimate resistance of the "effective shear area" A_{ev}, i.e. $R_{ev} = 0.6F_u A_{ev}$, where $A_{ev} = (A_{gv} + A_{nv})/2$ (A_{gv} and A_{nv} are the areas of the gross and net shear sections, see Fig. 4). The concept of the effective shear area was first proposed by Clements and Teh [69], based on the observation that the actual shear failure planes are between the net and gross shear planes. This basically agrees with the test observations of DSSBCs in this study (Fig. 6).

The analysis results indicated that the maximum loads reached by the tensile section ranged from 1.075 to 1.100R_{nt} for all the models. The actual maximum tensile load is higher than the theoretical value due to the triaxial stress state existed in the tensile section [70]. The maximum shear loads of the models ranged from 0.94 to 1.20R_{ev}. It should be noted that the tensile and shear loads corresponding to the ultimate connection load (referred to as ultimate tensile and shear loads, see Fig. 12) are always less than the maximum tensile and shear loads (also marked in Fig. 12). As shown in Fig. 12, the ultimate tensile load always lies on the post-peak branch, corresponding to a post-necking state of the tensile section. On the other hand, the ultimate shear load is always reached before attaining the maximum load. Fig. 13 shows the normalised ultimate tensile and shear loads ($R_{u,t}/R_{nt}$ and $R_{u,v}/R_{ev}$) of all the models, which are compared with those derived previously for ASSBCs [52]. The normalised ultimate tensile loads are plotted against the ratio of the summed lengths of the gross shear planes ($2L_c$) and the length of the gross tensile plane (p_2). The normalised ultimate shear loads, on the other hand, are plotted against the connection length normalised by the bolt hole diameter (L_c/d_0), where L_c is the connection length in the loading direction, equal to the length of a gross shear plane shown in Fig. 4.

As shown in Fig. 13(a), the normalised ultimate tensile load of DSSBCs decreases with the increase of $2L_c/p_2$. This can be explained by Fig. 12, where one can see that with longer shear planes and shorter tensile planes (greater $2L_c/p_2$), the difference of the displacements corresponding to the maximum tensile and shear loads tends to be greater. Consequently, the attainment of the ultimate tensile load (at a

Table 3
Summary of design parameters and analysis results of numerical models.

Thickness (mm)	Hole diameter d_o (mm)	Bolt	Number of bolt rows n_b	e_1 (mm)	p_1 (mm)	p_2 (mm)	Ultimate load R_{FEA} (kN)	Ultimate tensile load $R_{u,t}$ (kN)	Ultimate shear load $R_{u,v}$ (kN)
6	11	M10 G12.9	1	17	-	26	154.85	70.15	84.70
				24	-	26	190.62	70.46	120.16
				31	-	26	225.47	68.05	157.42
				24	-	33	222.90	103.35	119.55
6	11	M10 G12.9	2	17	24	26	251.97	68.76	183.21
				24	24	26	287.80	67.41	220.39
				31	24	26	322.06	66.86	255.20
				17	31	26	289.77	68.73	221.04
				24	31	26	325.21	65.47	259.74
				31	31	26	356.35	66.89	289.46
				17	24	33	291.77	101.81	189.96
				24	24	33	325.86	103.22	222.65
				31	24	33	360.11	101.54	258.56
				17	31	33	327.59	100.86	226.74
				24	31	33	361.28	98.94	262.34
				31	31	33	393.55	101.28	292.27
				17	24	40	326.53	135.85	190.68
				24	24	40	361.05	135.11	225.93
				31	24	40	395.51	135.38	260.13
				17	31	40	360.87	130.80	230.08
				24	31	40	394.89	132.47	262.42
				31	31	40	427.60	133.90	293.69
6	11	M10 G12.9	3	17	24	26	331.20	66.60	264.61
				24	24	26	383.21	65.64	317.56
				31	24	26	411.56	62.31	349.25
				17	31	26	416.31	66.92	349.39
				24	31	26	447.14	61.57	385.57
				31	31	26	478.42	63.53	414.89
				17	24	33	387.32	99.31	288.01
				24	24	33	417.96	100.16	317.80
				31	24	33	450.62	97.44	353.18
				17	31	33	453.08	100.46	352.62
				24	31	33	485.36	98.68	386.68
				31	31	33	516.44	100.18	416.26
				17	24	40	422.74	133.17	289.57
				24	24	40	455.99	133.98	322.01
				31	24	40	488.18	130.41	357.77
				17	31	40	487.12	133.69	353.43
6	11	M10 G12.9	3	24	31	40	519.81	132.19	387.62
				31	31	40	551.04	130.09	420.95
6	11	M10 G12.9	4	17	24	26	427.57	64.66	362.91
				24	24	26	461.27	64.01	397.25
				31	24	26	493.15	61.67	431.48
				17	31	26	527.82	65.04	462.78
				24	31	26	560.68	62.86	497.82
				31	31	26	590.72	62.56	528.16
				17	24	33	465.16	98.91	366.25
				24	24	33	499.53	98.55	400.98
				31	24	33	531.81	94.58	437.23
				17	31	33	565.51	99.99	465.52
				24	31	33	599.92	97.21	502.70
				31	31	33	631.24	95.65	535.59
				17	24	40	501.43	134.43	367.00
				24	24	40	537.67	133.23	404.44
				31	24	40	570.32	133.39	436.93
				17	31	40	600.40	132.02	468.37
				24	31	40	635.50	129.47	506.03
				31	31	40	668.69	130.41	538.28
6	11	M10 G12.9	5	17	24	26	508.88	65.86	443.02
				24	24	26	543.90	62.43	481.47
				31	24	26	574.62	60.62	514.01
				17	31	26	618.82	60.25	558.57
				24	31	26	645.08	61.95	583.13
				31	31	26	662.25	64.31	597.94
				17	24	33	547.29	99.07	448.22
				24	24	33	584.26	97.97	486.29
				31	24	33	615.76	97.31	518.45
				17	31	33	661.77	96.16	565.61
				24	31	33	688.81	95.44	593.37
				31	31	33	707.02	95.49	611.53
				17	24	40	584.13	132.43	451.70

(*continued on next page*)

Table 3 (*continued*)

Thickness (mm)	Hole diameter d_0 (mm)	Bolt	Number of bolt rows n_b	e_1 (mm)	p_1 (mm)	p_2 (mm)	Ultimate load R_{FEA} (kN)	Ultimate tensile load $R_{u,t}$ (kN)	Ultimate shear load $R_{u,v}$ (kN)
				24	24	40	622.14	132.19	489.95
				31	24	40	655.80	129.55	526.25
				17	31	40	699.56	127.87	571.69
				24	31	40	727.84	130.69	597.14
				31	31	40	746.60	130.87	615.74

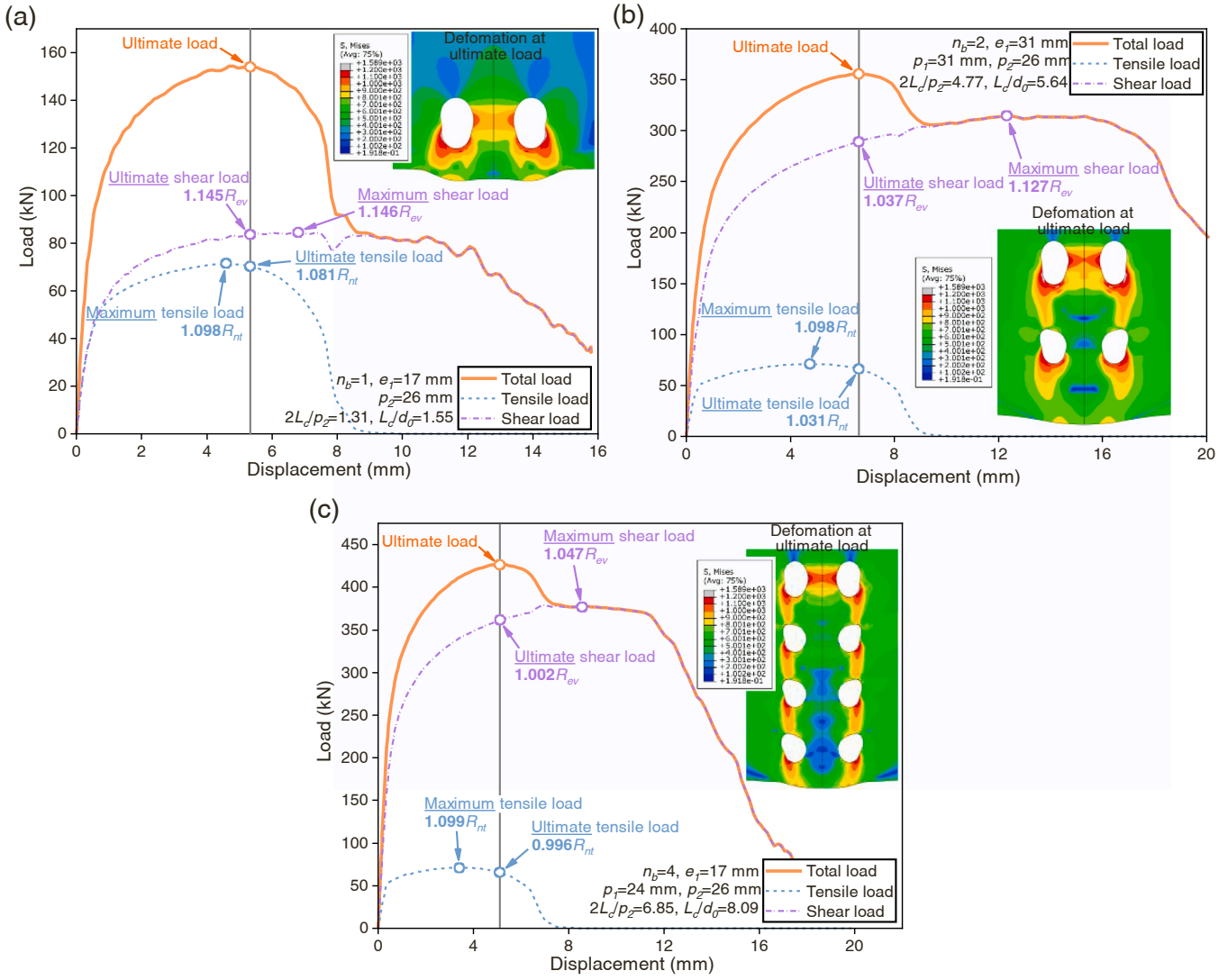

Fig. 12. Distribution of tensile and shear loads in DSSBCs.

displacement between those of maximum tensile and shear loads) is postponed in the post-necking range, which corresponds to a lower load level. Different from DSSBCs, the ASSBCs showed a decreasing trend of $R_{u,t}/R_{nt}$ with the decrease of $2L_c/p_2$ when $2L_c/p_2$ is less than 6 (see Fig. 13 (b)). This is due to the specific block shear mode (tensile yielding and shear cracking) of ASSBCs with relatively small $2L_c/p_2$, where the corresponding ultimate tensile load is attained in the pre-necking range. Overall, the ultimate tensile resistances of both ASSBCs and DSSBCs can be still reasonably estimated by $R_{nt} = F_u A_{nt}$.

As shown in Fig. 13(c), the normalised ultimate shear loads of DSSBCs and ASSBCs both decrease with the increase of connection length (L_c/d_0). This is easily understandable since the shear stress distribution is less uniform and the resultant average shear stress should be lower in longer connections. Compared with those of ASSBCs, the normalised ultimate shear loads of DSSBCs are significantly higher (and in most cases greater than 1). This is due to the much higher ultimate-to-yield strength ratio of austenitic stainless steel compared with DSS, which means full shear strain-hardening is more difficult to be achieved for ASSBCs (requiring larger shear displacements). For both ASSBCs and DSSBCs, the ultimate shear loads are remarkably higher than the theoretical yield resistance ($0.6F_yA_{ev}$), indicating significant shear strain-hardening at the ultimate load.

4. Design recommendations

4.1. Evaluation of existing methods

Numerous design methods are currently available for predicting the

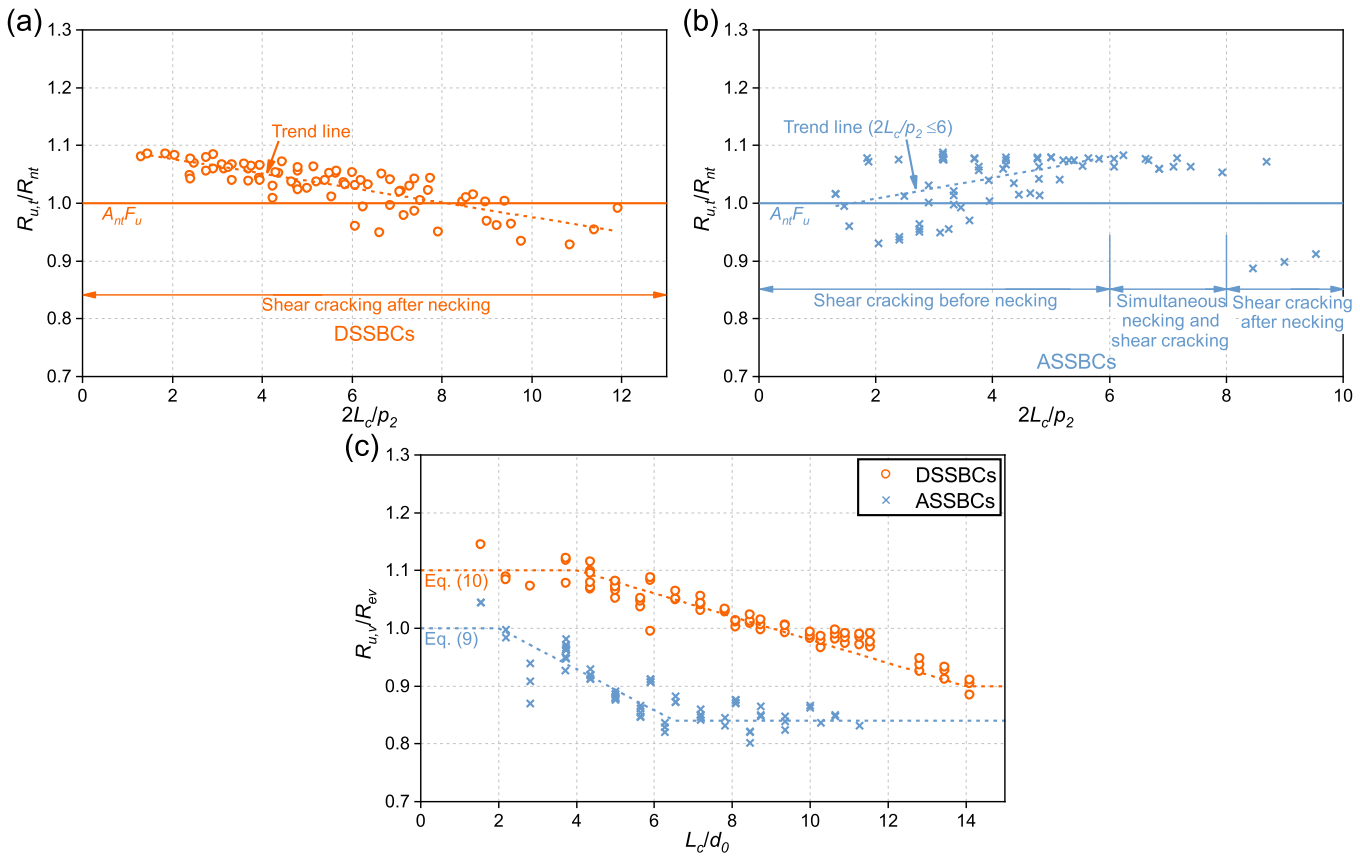

Fig. 13. Ultimate loads carried by tensile and shear sections: (a) ultimate tensile loads of DSSBCs; (b) ultimate tensile loads of ASSBCs [52]; (c) ultimate shear loads of ASSBCs [52] and DSSBCs.

Table 4
Summary of design methods and predictions for stainless steel bolted connections.

Method	Equation	R_n/R_{Test} or R_n/R_{FEA}							
		Test-ASSBC (9 tests)		FEA-ASSBC (70 models)		Test-DSSBC (11 tests)		FEA-DSSBC (76 models)	
		Mean	CoV	Mean	CoV	Mean	CoV	Mean	CoV
AISC 360[50]	$R_n = F_uA_{nt} + 0.6F_uA_{nv} \leq F_uA_{nt} + 0.6F_yA_{gv}$	0.631	7.1%	0.611	6.2%	0.800	3.4%	0.816	4.5%
CSA S16[64]	$R_n = \begin{cases} F_uA_{nt} + 0.6A_{gv}(F_u + F_y)/2 (F_y \leq 460MPa) \\ F_uA_{nt} + 0.6A_{gv}F_y (F_y > 460MPa) \end{cases}$	0.887	4.2%	0.934	4.0%	0.888	3.7%	0.911	5.0%
Hardash and Bjørhovde[59]	$R_n = F_uA_{nt} + 0.575A_{gv}F_{eff}$ $F_{eff} = (0.05 + 0.00185L_c)F_y + (0.95 - 0.00185L_c)F_u$	1.053	4.7%	1.022	2.9%	1.031	4.8%	1.057	5.2%
Topkaya[60]	$R_n = F_uA_{nt} + (0.25 + 0.35F_u/F_y - L_c/2800)F_yA_{gv}$	0.924	4.3%	0.906	3.5%	0.990	4.3%	1.009	4.8%
Teh and Uz[62]	$R_n = F_uA_{nt} + 0.6F_uA_{ev}$	1.007	4.4%	1.086	5.0%	0.947	3.0%	0.982	4.9%
Proposed	Eqs. (8)-(10)	0.977	3.0%	0.987	2.5%	1.002	2.3%	0.988	1.7%

Note: F_y—yield strength; F_u—ultimate strength; A_{nt}—area of net tensile section; A_{nv}—area of net shear sections; A_{gv}—area of gross shear sections; $A_{ev} = (A_{nv}+A_{gv})/2$—area of gross shear sections; L_c—connection length.

ultimate block shear resistance of bolted connections. Table 4 summarises five representative methods recommended in modern design codes [50,64] and research studies [59,60,62] for carbon steel bolted connections. As shown in Table 4, the equations of the five methods are similar regarding the tensile portion of the resistance, i.e., $R_{nt} = F_uA_{nt}$, which is identical with the theoretical resistance presumed in Section 3.4. The main differences are among the expressions of the ultimate shear resistance. For the method provided in AISC 360 [50] (also adopted in Eurocode 3 [51] and AS 4100 [65] with minor modifications), the ultimate shear resistance takes the lesser of those contributed by the theoretical ultimate capacity of the net shear sections ($0.6F_uA_{nv}$), and yield capacity of the gross shear sections ($0.6F_yA_{gv}$). The methods of CSA S16 [64], Hardash and Bjørhovde [59] and Topkaya [60] are based on a similar concept, which assumes that the gross shear sections (A_{gv}) would reach a stress level in between the yield ($0.6F_y$) and ultimate ($0.6F_u$) shear strengths, depending on the connection length and the strength of the material. The method of Teh and Uz [62] differs from the others for it assumes full strain-hardening of a predefined effective shear area ($0.6F_uA_{ev}$), which has been introduced in Section 3.4.

The ultimate resistance data of DSSBCs and ASSBCs [52] obtained from the tests and FEA (R_{Test} and R_{FEA}) were compared with the predictions (R_n) of the five design methods, as shown in Fig. 14(a)-(e). The overall performance of each method was evaluated by the mean ratio and CoV of R_n/R_{Test} or R_n/R_{FEA} for each set of data (test or FEA, ASSBC or DSSBC), which are summarised in Table 4. It was noticed that the method of AISC 360 [50] significantly underestimated the block shear resistance of SSBCs, especially ASSBCs. Since the ultimate tensile

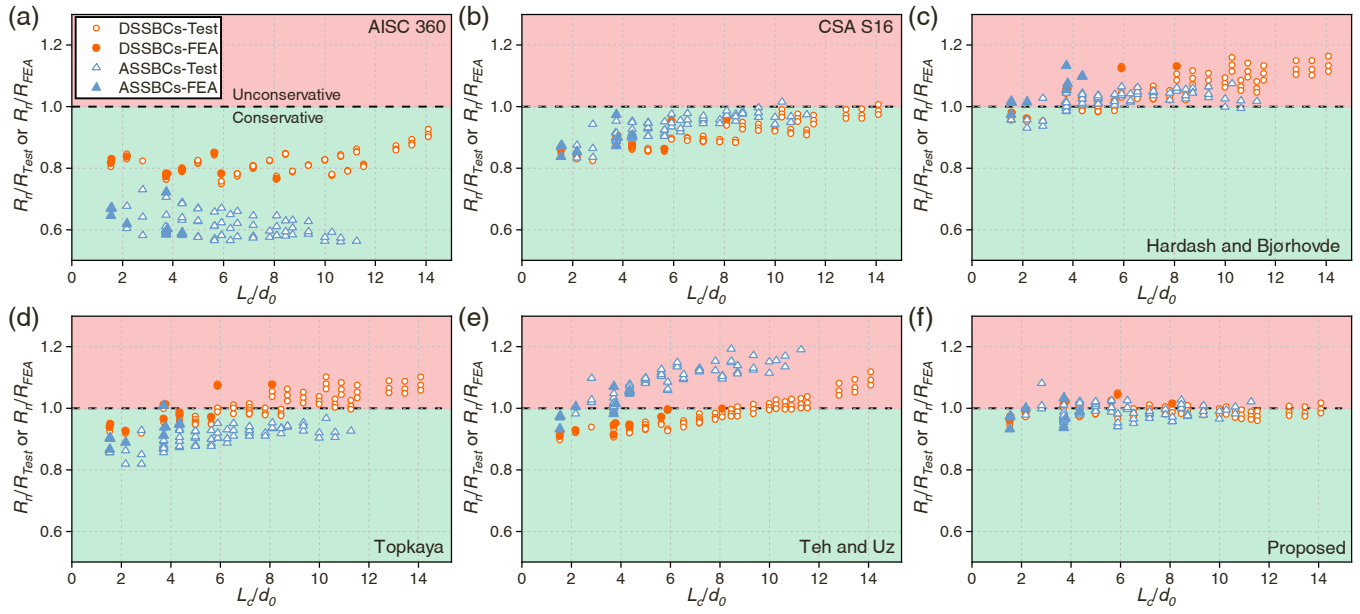

Fig. 14. Evaluation of block shear design methods for stainless steel bolted connections: (a) AISC 360 method [50]; (b) CSA S16 method [64]; (c) method of Hardash and Bjørhovde [59]; (d) method of Topkaya [60]; (e) method of Teh and Uz [62]; (f) proposed method.

resistances of both DSSBCs and ASSBCs are reasonably predicted by F_uA_{nt} (see Fig. 13(a) and (b)), it is apparent that the conservativeness of the AISC method is due to the assumption of either gross shear yielding ($0.6F_yA_{gv}$) or net shear fracture ($0.6F_uA_{nv}$) for stainless steel connections. The methods of CSA S16 [64], Hardash and Bjørhovde [59] and Topkaya [60] provided more accurate predictions than the AISC method. However, the shear failure area (gross shear area A_{gv}) assumed in these methods did not match the test observations in this and previous [52] studies, where the shear failure planes basically located between the net and gross shear planes. Moreover, as shown in Fig. 14(b)-(d), the accuracy of prediction seemed to be related to the material (ASSBC or DSSBC) and connection length (L_c/d_0) for these three methods. A similar problem was also noticed for the method of Teh and Uz [62], which assumes full strain-hardening of the effective shear area ($0.6F_uA_{ev}$). As shown in Fig. 14(e), the prediction of Teh and Uz becomes increasingly unconservative with the increase of connection length. Moreover, the predictions for ASSBCs are less conservative compared with those for DSSBCs. This trend agrees with that observed in Fig. 13(c), where the ultimate shear loads (normalised by $0.6F_uA_{ev}$) of ASSBCs are significantly lower than those of DSSBCs, both of which decrease with the increase of connection length.

4.2. Proposed design method for stainless steel bolted connections

To provide accurate and consistent predictions for both ASSBCs and DSSBCs, a modified block shear equation was developed, expressed in the form of:

$$R_n = F_uA_{nt} + F_{eff}A_{ev} \tag{8}$$

The proposed equation has a consistent tensile term (F_uA_{nt}) with the previous five methods. This is based on the analysed ultimate tensile loads shown in Fig. 13(a) and (b), which can be reasonably estimated by the theoretical ultimate resistance of the net tensile section. A more complex expression for the tensile term (e.g. the one proposed in Ref. [52] for ASSBCs) was deemed unnecessary for practical uses.

For the shear term, the method assumes failure across the effective shear sections ($A_{ev} = (A_{gv} + A_{nv})/2$). The effective strength F_{eff} of shear sections was derived based on the ultimate shear load data (Fig. 13(c)), which is dependent on the normalised connection length (L_c/d_0) and the material of the connection (ASSBC or DSSBC):

$$F_{eff} = 0.6k_vF_u + 0.6(1-k_v)F_y \tag{9}$$

$$k_v = \begin{cases} 1.108 - \dfrac{0.054L_c}{d_0}, 0.756 \le k_v \le 1 (ASSBC) \\ 1.714 - \dfrac{0.079L_c}{d_0}, 0.6 \le k_v \le 1.4 (DSSBC) \end{cases} \tag{10}$$

The predictions of Eqs. (8)-(10) are presented in Fig. 14(f), with the mean ratios and CoVs of R_n/R_{Test} (or R_n/R_{FEA}) summarised in Table 4. It is obvious that the accuracy of the proposed method is remarkably enhanced (with smaller CoVs and mean design-to-test/FEA ratios closer to 1) compared with the other methods. Moreover, the proposed method provides consistent predictions for all sets of data (test and FEA data of ASSBCs and DSSBCs).

4.3. Reliability analysis

The reliability of the proposed design method was evaluated following the procedure specified in EN 1990 [71] and ANSI/AISC 370–21 [72]. Table 5 summarises the key statistical parameters and results of the reliability analysis according to EN 1990 [71] with a reliability index of 3.8 for ultimate limit state design and a reference period of 50 years. Based on the recommendation of Afshan et al. [73], the over-strength factors for yield strength were taken as 1.3 and 1.1 respectively for austenitic and duplex stainless steels; whilst the over-strength factor for ultimate strength was taken as 1.1 for both materials. The CoVs of yield strength (V_{fy}) and ultimate strength (V_{fu}) were 0.06 and 0.035 respectively for austenitic stainless steel, and 0.03 and 0.035 for DSS [73]. The CoV of geometric properties ($V_{geometry}$) was taken as 0.05 for both materials [73]. Based on a total of 166 test/FEA data (79 ASSBCs, 87 DSSBCs), the mean correction factor b for the proposed design method was calculated as 1.011 and 1.012 for ASSBCs and DSSBCs. The CoVs of the test/FEA data relative to the design prediction were 0.025 for ASSBCs and 0.018 for DSSBCs. The resultant partial safety factors (γ_M*) were calculated as 1.153 and 1.162 for ASSBCs and DSSBCs respectively. These results indicate that that the partial factor γ_{M2} in Eurocode 3 [48,51] (1.25) can be safely used with the proposed block shear method for ASSBCs and DSSBCs.

Table 6 shows the key statistical parameters and results derived from the reliability analysis based on ANSI/AISC 370–21 [72], with a targeted

Table 5
Parameters and results of reliability analysis according to EN 1990.

Material	No. of test or FEA data	Over-strength factor for F_y	Over-strength factor for F_u	V_{fy}	V_{fu}	$V_{geometry}$	b	V_δ	V_r	$\gamma_M{}^*$
Austenitic	79	1.3	1.1	0.06	0.035	0.05	1.011	0.025	0.089	1.153
Duplex	87	1.1	1.1	0.03	0.035	0.05	1.012	0.018	0.089	1.162

Table 6
Parameters and results of reliability analysis according to ANSI/AISC 370–21.

Material	No. of tests/FEA data	P_m	V_R	V_Q	β	ϕ^*
Austenitic	79	1.013	0.069	0.19	4.0	0.74
Duplex	87	1.011	0.067	0.19	4.0	0.74

reliability index (β) of 4.0 for connections specified in terms of Load and Resistance Factor Design (LRFD). The professional factor (P_m), which represents the mean ratio of R_{Test} or R_{FEA} to the predicted resistance (R_n) based on the proposed design equations, was found to be 1.013 and 1.011 for ASSBCs and DSSBCs, respectively. The CoV for resistance (V_R) was calculated as 0.069 and 0.067 for ASSBCs and DSSBCs, respectively. Besides, the CoV of the load effect V_Q was taken as 0.19 for both materials assuming a dead load-to-live load ratio of 1:3 [72]. The resultant resistance factor (ϕ^*) was calculated as 0.74 for both ASSBCs and DSSBCs, which is marginally lower than the specified value of 0.75 in ANSI/AISC 370–21 [72]. It is hence recommended to utilise a resistance factor of 0.70 in conjunction with the proposed block shear method for ASSBCs and DSSBCs for safety considerations.

5. Conclusions

This paper has presented an experimental and numerical study on the block shear behaviour of duplex stainless steel bolted connections (DSSBCs). It was observed that the only block shear failure mode of DSSBCs was necking of the net tensile section and yielding of the effective shear sections (lying between the net and gross shear sections), which is consistent with that of carbon steel bolted connections. The block shear behaviour of DSSBCs differed significantly from that of austenitic stainless steel bolted connections (ASSBCs), which exhibited three different block shear modes depending on the bolt arrangement.

The block shear behaviour of DSSBCs can be accurately simulated by the finite element analysis (FEA), with a Hill yield criterion accounting for the anisotropic mechanical properties of duplex stainless steel (DSS). A further analysis of the FE results of DSSBCs revealed that the ultimate load carried by the tensile section can be reasonably estimated by the product of ultimate strength (F_u) and the net tensile area (A_{nt}). On the other hand, the ultimate load carried by the shear sections can be higher than the theoretical ultimate capacity of the effective shear area ($0.6F_uA_{ev}$). Compared with ASSBCs, DSSBCs exhibited higher levels of shear strain-hardening at the ultimate state.

The test and FEA data were used to evaluate the performances of existing design methods. It was noted that the method specified in most of the existing design codes (AISC 360, Eurocode 3 and AS 4100) significantly underestimated the block shear capacity of stainless steel bolted connections (SSBCs), especially ASSBCs. The other methods that assumed partial or full strain-hardening of the shear sections achieve better predictions of the block shear capacity of SSBCs. However, inconsistent predictions were obtained for ASSBCs and DSSBCs due to the different shear strain-hardening behaviour.

Based on available test and FEA data, a modified block shear design method was proposed for predicting the ultimate block shear capacity of ASSBCs and DSSBCs. The ultimate load of the tensile section is predicted by F_uA_{nt}, whilst the stress level of the effective shear area is related to the material (austenitic or duplex) and connection length. The proposed method showed an improved and consistent accuracy for ASSBCs and DSSBCs. Based on the results of reliability analyses, it is shown that a partial factor of 1.25 (in accordance with the EN 1990 method) and a resistance factor of 0.70 (in accordance with ANSI/AISC 370–21) can be safely adopted for the proposed method.

CRediT authorship contribution statement

Song Yuchen: Conceptualization, Formal analysis, Investigation, Methodology, Visualization, Writing – original draft. **Ke Ke:** Resources, Writing – review & editing. **Lin Xue-Mei:** Funding acquisition, Investigation, Methodology, Visualization, Writing – review & editing. **Yam Michael C.H.:** Conceptualization, Funding acquisition, Project administration, Resources, Supervision, Writing – review & editing. **Wang Jia:** Funding acquisition, Writing – review & editing.

Declaration of Competing Interest

There is no financial/personal interest or belief that could affect our objectivity. There are no potential conflicts of interest either.

Data Availability

Data will be made available on request.

Acknowledgement

This work received supports from the Chinese National Engineering Research Centre (CNERC) for Steel Construction (Hong Kong Branch) at The Hong Kong Polytechnic University (Grant No.: BBVW), the Guangdong Basic and Applied Basic Research Foundation (Grant No.: 2022A1515110057), as well as the National Natural Science Foundation of China (Grant No.: 52008093 and 52378137).

References

[1] Charles J. Duplex stainless steels - a review after DSS '07 held in Grado. Steel Res Int 2008;79(6):455–65.
[2] Theofanous M, Gardner L. Testing and numerical modelling of lean duplex stainless steel hollow section columns. Eng Struct 2009;31(12):3047–58.
[3] Blog Sagrada Família, Stainless steel at the Sagrada Família: what do we use it for? (2018), https://blog.sagradafamilia.org/en/specialists/stainless-steel/.
[4] T. Vejrum, D.W. Bergman, N. Yeung, Stonecutters bridge, Hong Kong: design and construction of the composite upper tower in stainless steel, NSCC2009 2009.
[5] Errera SJ, Popowich DW, Winter G. Bolted and welded stainless steel connections. J Struct Div ASCE 1974;100(6):1279–96.
[6] Ryan I. Dev Use Stainl Steel Constr WP 1999;4:2.
[7] Bouchaïr A, Averseng J, Abidelah A. Analysis of the behaviour of stainless steel bolted connections. J Constr Steel Res 2008;64(11):1264–74.
[8] Salih EL, Gardner L, Nethercot DA. Bearing failure in stainless steel bolted connections. Eng Struct 2011;33(2):549–62.
[9] Salih EL, Gardner L, Nethercot DA. Numerical investigation of net section failure in stainless steel bolted connections. J Const Steel Res 2010;66(12):1455–66.
[10] Jiang K, Zhao O. Experimental and numerical studies of stainless steel angle-to-plate connections. Thin-Walled Struct 2022;173:109026.
[11] Jiang K, Zhao O, Young B. Experimental and numerical study of stainless steel channel-to-gusset plate connections. Eng Struct 2022;265:114461.
[12] Jiang K, Zhao O. Unified machine-learning-assisted design of stainless steel bolted connections. J Constr Steel Res 2023;211:108155.
[13] Kim TS, Cho TJ. Influence of microstructure difference of stainless steels on the strength and fracture of bolted connections. ISIJ Int 2013;53(2):365–74.
[14] Lim J-S, Kim T-S, Kim S-H. Ultimate strength of single shear bolted connections with cold-formed ferritic stainless steel. J Zhejiang U Sci A 2013;14(2):120–36.
[15] Kim GY, Kim TS, Hwang BK, Kim JS. Ultimate strength of lean duplex stainless steel single-shear bolted connections with four bolts. Thin-Walled Struct 2020;155:106950.
[16] Kim TS, Hong SK, Hwang BK, Kim JS. Block shear capacity in cold-formed lean duplex stainless steel double-shear bolted connections. Thin Wall Struct 2021;161:107520.

[17] Talja A, Torkar M. Lap shear tests of bolted and screwed ferritic stainless steel connections. Thin Wall Struct 2014;83:157–68.
[18] Cai Y, Young B. Structural behavior of cold-formed stainless steel bolted connections. Thin Wall Struct 2014;83:147–56.
[19] Cai Y, Young B. Carbon steel and stainless steel bolted connections undergoing unloading and re-loading processes. J Const Steel Res 2019;157:337–46.
[20] Cai Y, Young B. Experimental investigation of carbon steel and stainless steel bolted connections at different strain rates. Steel Compos Struct 2019;30(6):551–65.
[21] dos Santos JJ, Liang Y, Zhao O, de Andrade SAL, de Lima LRO, Gardner L, et al. Testing and design of stainless steel staggered bolted connections. Eng Struct 2021;231:111707.
[22] Sobrinho KP, da Silva AT, Rodrigues MC, Henriques JA, Vellasco PCGS, de Lima LRO. A comprehensive assessment of curling effects in stainless steel bolted connections. Thin Wall Struct 2022;176:109387.
[23] Jiang K, Zhao O. Ferritic stainless steel thin sheet bolted connections failing by bearing–curling interaction: Testing, modelling and design. Eng Struct 2023;283:115919.
[24] Kim TS, Kuwamura H. Finite element modeling of bolted connections in thin-walled stainless steel plates under static shear. Thin Wall Struct 2007;45(4):407–21.
[25] Cai Y, Young B. Behavior of cold-formed stainless steel single shear bolted connections at elevated temperatures. Thin Wall Struct 2014;75:63–75.
[26] Cai Y, Young B. Bearing factors of cold-formed stainless steel double shear bolted connections at elevated temperatures. Thin Wall Struct 2016;98:212–29.
[27] Cai Y, Young B. High temperature tests of cold-formed stainless steel double shear bolted connections. J Const Steel Res 2015;104:49–63.
[28] Song Y, Wang J, Uy B, Li D. Experimental behaviour and fracture prediction of austenitic stainless steel bolts under combined tension and shear. J Constr Steel Res 2020;166:105916.
[29] Song Y, Wang J, Uy B, Li D. Stainless steel bolts subjected to combined tension and shear: behaviour and design. J Constr Steel Res 2020;170:106122.
[30] Stranghöner N, Abraham C. Shear resistance of austenitic and duplex stainless steel bolts. J Constr Steel Res 2021;184:106807.
[31] Stranghöner N, Abraham C. Tension and interaction resistance of austenitic and duplex stainless steel bolts, J. Const. Steel Res 2022;198:107536.
[32] Stranghöner N, Afzali N, de Vries P, Schedin E, Pilhagen J. Slip factors for slip-resistant connections made of stainless steel. J Constr Steel Res 2019;152:235–45.
[33] Zheng B, Wang J, Gu Y, Shu G, Xie J, Jiang Q. Experimental study on stainless steel high-strength bolted slip-resistant connections. Eng Struct 2021;231:111778.
[34] Dobrić J, Cai Y, Young B, Rossi B. Behaviour of duplex stainless steel bolted connections. Thin Wall Struct 2021;169:108380.
[35] Hasan MJ, Ashraf M, Uy B. Moment-rotation behaviour of top-seat angle bolted connections produced from austenitic stainless steel. J Const Steel Res 2017;136:149–61.
[36] Hasan MJ, Al-Deen S, Ashraf M. Behaviour of top-seat double web angle connection produced from austenitic stainless steel. J Constr Steel Res 2019;155:460–79.
[37] Elflah M, Theofanous M, Dirar S, Yuan H. Behaviour of stainless steel beam-to-column joints-Part 1: Experimental investigation. J Constr Steel Res 2019;152:183–93.
[38] Elflah M, Theofanous M, Dirar S. Behaviour of stainless steel beam-to-column joints-Part 2: Numerical modelling and parametric study. J Constr Steel Res 2019;152:194–212.
[39] Elflah M, Theofanous M, Dirar S, Yuan H. Structural behaviour of stainless steel beam-to-tubular column joints. Eng Struct 2019;184:158–75.
[40] Bu Y, Wang Y, Zhao Y. Study of stainless steel bolted extended end-plate joints under seismic loading. Thin-Walled Struct 2019;144:106255.
[41] Gao JD, Yuan HX, Du XX, Hu XB, Theofanous M. Structural behaviour of stainless steel double extended end-plate beam-to-column joints under monotonic loading. Thin-Walled Struct 2020;151:106743.
[42] Gao JD, Du XX, Yuan HX, Theofanous M. Hysteretic performance of stainless steel double extended end-plate beam-to-column joints subject to cyclic loading. Thin-Walled Struct 2021;164:107787.
[43] Song Y, Wang J, Uy B, Li D. Behaviour and design of stainless steel-concrete composite beam-to-column joints. J Constr Steel Res 2021;184:106800.
[44] Song Y, Uy B, Li D, Wang J. Ultimate behaviour and rotation capacity of stainless steel end-plate connections. Steel Compos Struct 2022;42(4):569–90.
[45] Cai Y, Young B. Structural behavior of cold-formed stainless steel bolted connections. Thin-Walled Struct 2014;83:147–56.
[46] Yang L, Wang Y, Guan J, Zhang Y, Shi Y. Bearing strength of stainless steel bolted connections. Adv Struct Eng 2015;18(7):1051–62.
[47] EN 1993-1-3. Eurocode 3: Design of steel structures, Part 1-3: General rules-Supplementary rules for cold-formed members and sheeting. Comité Européen de Normalisation. Belgium: Brussels; 2007.
[48] EN1993-1-4. Eurocode 3: Design of Steel Structures, Part 1-4: General rules-Supplementary rules for stainless steels. Comité Européen de Normalisation. Belgium: Brussels; 2015.
[49] Structural Stainless Steel. American Institute of Steel Construction. Chic, USA 2013.
[50] AISC 360. Specification for Structural Steel Buildings. American Institute of Steel Construction, Chicago. USA: Illinois,; 2016.
[51] EN. 1-8, Eurocode 3: Design of Steel Structures, Part 1-8: Design of Joints. Comité Européen de Normalisation. Belgium: Brussels; 1993. p. 2021.
[52] Song Y, Lin X-M, Yam MCH, Ke K. Block shear failure of austenitic stainless steel bolted connections. Thin-Walled Struct 2023;193:111251.
[53] ASTM E8/E8M, Standard Test Methods for Tension Testing of Metallic Materials, ASTM, PA, USA, 2016.
[54] Huang Y, Young B. The art of coupon tests. J Constr Steel Res 2014;96:159–75.
[55] Hutchinson WB, Ushioda K, Runnsjö G. Anisotropy of tensile behaviour in a duplex stainless steel sheet. Mater Sci Tech 1985;1(9):728–36.
[56] Saliba N, Gardner L. Cross-section stability of lean duplex stainless steel welded I-sections. J Constr Steel Res 2013;80:1–14.
[57] Song Y. Behaviour and design of stainless steel and stainless steel-concrete composite beam-to-column joints with end-plate connections. Univ Syd 2023.
[58] Lin X-M, Yam MCH, Ke K, He Q, Chung K-F. Investigation of block shear strength of high strength steel bolted connections, J. Const. Steel Res 2022;196:107407.
[59] Hardash SG, Bjorhovde R. Gusset plate design utilizing block-shear concepts. Univ Ariz 1984.
[60] Topkaya C. A finite element parametric study on block shear failure of steel tension members. J Const Steel Res 2004;60(11):1615–35.
[61] Teh LH, Clements DDA. Block shear capacity of bolted connections in cold-reduced steel sheets. J Struct Eng 2012;138(4):459–67.
[62] Teh LH, Uz ME. Block shear failure planes of bolted connections - Direct experimental verifications. J Const Steel Res 2015;111:70–4.
[63] Jiang K, Tan KH, Zhao O, Gardner L. Block tearing of S700 high strength steel bolted connections: Testing, numerical modelling and design. Eng Struct 2021;246:112979.
[64] CSA S16–19, Design of steel structures, Canadian Standards Association, Ontario, Canada, 2019.
[65] AS 4100–2020, Steel structures, Standards Australia, Sydney, Australia, 2020.
[66] ABAQUS, User's Manual, Version. Dassault Systemes Corp., Providence. USA: RI; 2016. p. 2016.
[67] Lee YW, Wierzbicki T. Quick fracture calibration for industrial use. Impact and Crashworthiness Laboratory. Massachusetts Institute of Technology,; 2004.
[68] Hill R, Orowan E. A theory of the yielding and plastic flow of anisotropic metals. Proc R Soc Lond Ser A Math Phys Sci 1948;193(1033):281–97.
[69] Clements DDA, Teh LH. Active shear planes of bolted connections failing in block shear. J Struct Eng 2013;139(3):320–7.
[70] Lin X-M, Yam MCH, Chung K-F, Lam ACC. A study of net-section resistance of high strength steel bolted connections. Thin-Walled Struct 2021;159:107284.
[71] BS EN 1990: 2002+A1: 2005, Eurocode-Basis of structural design, Comité Européen de Normalisation, Brussels, Belgium, 2005.
[72] ANSI/AISC 370–21, Specification for Structural Stainless Steel Buildings, American Institute of Steel Construction, Chicago, Illinois, USA, 2021.
[73] Afshan S, Francis P, Baddoo NR, Gardner L. Reliability analysis of structural stainless steel design provisions. J Const Steel Res 2015;114:293–304.
[74] Song Y, Yam MCH, Wang J. Enhanced progressive collapse resistance of bolted beam-to-column connections with ductile stainless steel components. Eng Struct 2023;275:115337.